Suppression of writing error in a spin-orbit magnetization switching device using fieldlike torque

Tomohiro Taniguchi*
National Institute of Advanced Industrial Science and Technology (AIST),
Research Institute for Hybrid Functional Integration, Tsukuba, Ibaraki 305-8568, Japan

(Received 21 April 2025; revised 3 June 2025; accepted 23 June 2025; published 7 July 2025)

Spin-orbit torque (SOT) induced magnetization switching has attracted attention because of its applicability to a fast writing method in nonvolatile memory. However, it has been clarified that the magnetization switching is sensitive to the current density, the magnetic field strength, and the initial condition, even at zero temperature due to back switching, where the magnetization moves close to the switched state in the presence of SOT but is back to the initial state after turning off the current. Here, we study the SOT-driven magnetization switching probability at finite temperature through numerical simulation of the Landau-Lifshitz-Gilbert equation. The switching probability decreases as the electric current density increases, which is in contrast to that found in the conventional spin-transfer torque devices. The decrease of the switching probability originates from the combination of the back switching and thermal fluctuation. It is found that the switching probability can be kept high when fieldlike torque with an appropriate value is introduced. The analysis on the temporal dynamics indicates that the presence of the fieldlike torque leads to an effective enhancement of the damping torque and results in a fast relaxation to the switched state, which helps to avoid the back switching.

DOI: 10.1103/yngx-z13v

I. INTRODUCTION

Magnetization switching driven by spin-orbit torque (SOT) has attracted attention to manipulate the magnetization in ferromagnets in nanometer scales [1–3]. SOT originates from spin current generated by spin-orbit interaction in nonmagnetic electrodes [4–6]. SOT causes a destabilization of a perpendicularly magnetized ferromagnet in nanoseconds scale, which is faster than that caused by spin-transfer torque (STT) [7,8] in the conventional two-terminal structures [9–15]. Therefore, the SOT driven magnetization manipulation is expected to be a writing method for next-generation magnetoresistive random access memory (MRAM) [16]. However, the SOT driven magnetization switching requires an additional factor for reliable switching. This is because the direction of SOT is orthogonal to the easy axis of the perpendicularly magnetized ferromagnet, and thus, SOT cannot choose the relaxed state of the magnetization after turning off the current deterministically. In the first studies of SOT, applied magnetic field pointing to an in-plane direction was used for realizing the deterministic switching [1,2]. After that, various approaches for magnetic field-free switching have been proposed, such as utilizing lateral structure asymmetry [17], tilted magnetic anisotropy [18,19], exchange bias from the antiferromagnet [20], interlayer exchange coupling [21], STT assistance [22,23], and SOT from a ferromagnetic electrode [24–27]. In this work, we focus on the originally proposed method, i.e., using an in-plane applied magnetic field. This is because this method is still used widely and provides a fundamental but useful insight for understanding the SOT driven magnetization switching.

The previous works have revealed that the magnetization switching assisted by the in-plane applied magnetic field becomes sensitive to the system parameters [28,29]. This is because the magnetization starts to precess around the applied magnetic field after turning off the current, and therefore, it possibly returns to the initial state; therefore, the switching is failed. The phenomenon appears both perpendicularly [28,29] and in-plane [30,31] magnetized ferromagnets and was named as back switching [31]. The back switching causes the switching error and reduces the reliability of SOT-MRAM. It would be desirable to investigate methods to overcome the issues related to the back switching.

In this work, we study the effect of the back switching on the SOT-driven magnetization switching by numerically solving the Landau-Lifshitz-Gilbert (LLG) equation. Note that our previous work [29] already clarified a condition on the system parameters to avoid the back switching at zero temperature. We, however, notice that the back switching appears even for such a set of parameters at finite temperature so there are thermal fluctuations. It is shown that the switching probability decreases as the electric current density increases. This is in contrast to the conventional STT switching, where the switching probability increases monotonically. It is found that the high switching probability can be recovered when fieldlike torque is introduced. We find from the analysis of the magnetization dynamics that this recovery of the switching probability is due to an effective enhancement of the damping torque by the SOT in the presence of the fieldlike torque.

The paper is organized as follows. In Sec. II, we provide the system description. In Sec. III, we show the current dependence of the switching probability. We also investigate the

*Contact author: tomohiro-taniguchi@aist.go.jp

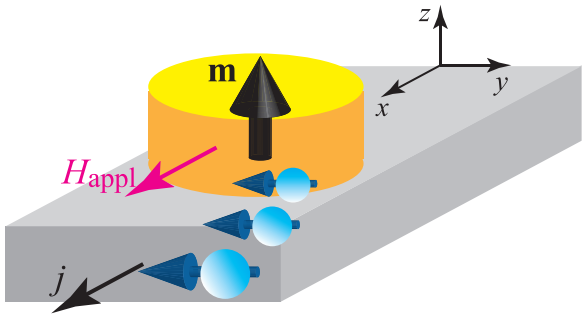

FIG. 1. Schematic illustration of SOT devices. Electric current density j flowing in a bottom nonmagnet in the x direction generates spin current polarized in the y direction, which is injected into a ferromagnet placed on the nonmagnet. The spin current exerts SOT on magnetization $\mathbf{m}$ and changes its direction with help of an applied magnetic field $H_{\rm appl}$ in the x direction.

effect of the fieldlike torque on the magnetization switching. In Sec. IV, the switching probability for a shorter current pulse is evaluated. Section V is devoted to the conclusion.

II. SYSTEM DESCRIPTION

In this section, we first describe the system under study and show characteristic currents of the magnetization dynamics at zero temperature.

A. LLG equation

Figure 1 is a schematic illustration of the system. A ferromagnetic free layer is placed on a bottom nonmagnetic electrode. By applying electric current density j flowing in the x direction to the bottom nonmagnetic electrode, spin current polarized in the y direction is generated and is injected into the ferromagnetic free layer. This spin current exerts SOT acting on the magnetization in the free layer, which is described by the LLG equation (see also Appendix A for the method solving the LLG equation),

$$\frac{d\mathbf{m}}{dt} = -\gamma\mathbf{m}\times(\mathbf{H}+\mathbf{h}) - \gamma H_{\rm s}\mathbf{m}\times(\mathbf{e}_y\times\mathbf{m}) - \beta\gamma H_{\rm s}\mathbf{m}\times\mathbf{e}_y + \alpha\mathbf{m}\times\frac{d\mathbf{m}}{dt}, \tag{1}$$

where $\mathbf{m}$ is the unit vector pointing in the magnetization direction in the free layer, while $\mathbf{e}_k$ $(k = x, y, z)$ is a unit vector in the k direction. The parameters γ and α are the gyromagnetic ratio and the Gilbert damping constant, respectively. The magnetic field consists of a time-independent applied magnetic field $H_{\rm appl}$ in the x direction and the perpendicular magnetic anisotropy field $H_{\rm K}(>0)$ in the z direction as

$$\mathbf{H} = H_{\rm appl}\mathbf{e}_x + H_{\rm K}m_z\mathbf{e}_z. \tag{2}$$

For convenience, we assume that $H_{\rm appl} > 0$ and $|H_{\rm appl}/H_{\rm K}| < 1$. The magnetization then has two energetically stable (minimum energy) states at $\mathbf{m}_{\rm s\pm} = (\sin\theta_{\rm s}, 0, \pm\cos\theta_{\rm s})$ with $\theta_{\rm s} = \sin^{-1}(H_{\rm appl}/H_{\rm K})$. The strength of SOT is given by

$$H_{\rm s} = \frac{\hbar\vartheta j}{2eMd}, \tag{3}$$

TABLE I. Parameters used in the numerical calculations: M, saturation magnetization; $H_{\rm K}$, perpendicular magnetic anisotropy field; γ, gyromagnetic ratio; α, Gilbert damping constant; d, thickness of the free layer; V, volume of the free layer; ϑ, spin Hall angle; $H_{\rm appl}$: applied magnetic field.

Quantity	Value
M	1500 emu/cm^3
$H_{\rm K}$	1.172 kOe
γ	1.764×10^7 rad/(Oe s)
α	0.030
d	1 nm
V	$d\times\pi\times30^2$ nm^3
ϑ	0.30
$H_{\rm appl}$	400 Oe

where ϑ is the spin Hall angle while M and d are the saturation magnetization and the thickness of the free layer. The dimensionless parameter β is the ratio between the dampinglike and fieldlike SOTs. Recall that the fieldlike torque in STT devices originates from the spin-dependent interfacial scattering or the spin precession inside the ferromagnet [32–34] and is often small. The fieldlike torque in SOT devices, on the other hand, may additionally originate from an interfacial spin-orbit effect and can be large [35]. The parameter β can be either positive or negative, depending on the material combination of the nonmagnetic electrode and the ferromagnetic free layer [36–41]. For example, the harmonic voltage measurement in Ta/CoFeB/MgO heterostructure indicates a presence of positive β [36], while a negative β is necessary to explain the switching experiment of an in-plane W/CoFeB/MgO based SOT-MRAM [41]. The effect of the fieldlike torque on the magnetization dynamics was investigated in Refs. [42,43] numerically, however, the calculations were limited to zero temperature. The component h_k $(k = x, y, z)$ of the random field $\mathbf{h}$ due to the thermal fluctuation satisfies the fluctuation-dissipation theorem [44],

$$\langle h_k(t)h_\ell(t')\rangle = \frac{2\alpha k_{\rm B}T}{\gamma MV}\delta_{k\ell}\delta(t-t'), \tag{4}$$

where V is the volume of the ferromagnet. For convenience, we assume that the initial state of the magnetization is $\mathbf{m}_{\rm s+}$; therefore, the magnetization switching in this work corresponds to the motion of the magnetization from a state near $\mathbf{m}_{\rm s+}$ to a state near $\mathbf{m}_{\rm s-}$. We solve the LLG equation at finite temperature 10^7 times with different random number to estimate the switching probability. In each trial, we firstly solve the LLG equation without SOT with the initial condition $\mathbf{m} = \mathbf{m}_{\rm s+}$ for 10 ns to generate natural initial condition at finite temperature. Next, we solve the LLG equation with SOT with the pulse width of $t_{\rm p}$, and then, solve the LLG equation without SOT 10 ns to estimate the relaxed state. When $m_z < (\geqslant)0$ at this final time, the trial is regarded as a switched (nonswitched) case. The values of the parameters are summarized in Table I [45]. Here $H_{\rm K}$ is set such that the thermal stability $\Delta_0 = MH_{\rm K}V/(2k_{\rm B}T)$, with the temperature T at room temperature ($T = 300$ K), is equal to 60. Recall that the magnetization dynamics obtained from Eq. (1) can be represented as a trajectory on a unit sphere because the LLG

equation conserves the norm (magnitude) of the magnetization. This fact will be used to describe the solution of Eq. (1) in the following.

B. Characteristic currents

It should be recalled that there are two characteristic currents characterizing the SOT driven magnetization switching in a perpendicularly magnetized ferromagnet [28,29]. The first one is the critical current density j_c given by

$$j_c = \frac{2eMd}{\hbar\vartheta} H_K \frac{-3\frac{H_{appl}}{H_K} + \sqrt{8 + \left(\frac{H_{appl}}{H_K}\right)^2}}{16} \times \sqrt{8 - 2\frac{H_{appl}}{H_K}\left[\frac{H_{appl}}{H_K} + \sqrt{8 + \left(\frac{H_{appl}}{H_K}\right)^2}\right]}. \quad (5)$$

When the current density exceeds the critical value j_c, i.e., when $j/j_c > 1$, the magnetization pointing near the initial state ($\mathbf{m} = \mathbf{m}_{s+}$) is destabilized by the SOT and moves to the negative m_z region [28]; see also Appendix B for the applicability of Eq. (5). However, it is not guaranteed that the magnetization relaxes to the switched state ($\mathbf{m} = \mathbf{m}_{s-}$) after turning off the electric current density. This is because the magnetization starts to precess around the in-plane magnetic field and possibly returns to the initial state. The phenomenon was named back switching in Ref. [31]; see also Sec. III B and Appendix B for the detailed explanation of the back switching. It was found that the back switching can be avoided when the electric current density is below the second characteristic current density, named threshold current density for the reliable switching defined by [29]

$$j_{th} = \frac{2eMd}{\hbar\vartheta} H_{appl} \sqrt{\frac{2}{-\left(\frac{H_{appl}}{H_K}\right)^2 + \frac{H_{appl}}{H_K}\sqrt{4 + \left(\frac{H_{appl}}{H_K}\right)^2}}}. \quad (6)$$

Summarizing them, the magnetization relaxes to the switched state ($\mathbf{m}_{s-}$) after turning off the current when the current density j satisfies $j/j_c > 1$ and $j/j_{th} < 1$. On the other hand, when $j/j_{th} > 1$, whether the magnetization relaxes to $\mathbf{m}_{s+}$ or $\mathbf{m}_{s-}$ after turning off the current sensitively depends on the values of the parameters [29]. Note that the formulas of j_c and j_{th} are derived from the LLG equation at zero temperature, where the fieldlike torque is neglected. For the present parameters, j_c and j_{th} are estimated to be 49 MA/cm^2 and 113 MA/cm^2, respectively, i.e., $j_{th}/j_c \simeq 2.3$.

In the following calculations, we mainly focus on the current region of $j/j_c \leqslant 2.0$. Therefore, at zero temperature, the back switching does not occur, and the magnetization switching is achieved (see also Appendix B). However, the presence of the thermal fluctuation leads to the switching error, as shown below.

C. Pulse width and current range

One of the motivations for developing SOT-MRAM is to achieve a fast writing within one nanosecond [46–48]. Thus, one might be interested in the switching probability for a short pulse width. From a theoretical viewpoint, however, it is useful to assume relatively long pulse width. For example, the magnetization may reach a steady state point when the pulse width is sufficiently long; in this case, an analytical solution of the LLG equation may be obtained, which helps to reveal the underlying physics in the switching process. Thus, we firstly use a relatively long pulse width ($t_p = 5$ ns) in Sec. III to clarify the switching process and then, use a relatively short pulse width ($t_p = 1$ ns) in Sec. IV for readers interested in practical applications.

The SOT driven magnetization switching probability was already investigated in Ref. [49], where the current range is $h_s \leqslant 0.5$ (h_s in Ref. [49] is H_s/H_K in the present work), which corresponds to $j/j_c \lesssim 1$ in the limit of $H_{appl} \ll H_K$. The switching for $j/j_c < 1$ corresponds to the thermally activated switching and requires the long current pulse because the assist from the thermal fluctuation is necessary. On the other hand, we mainly focus on the dynamical switching ($j/j_c \gtrsim 1.0$) because the fast switching is of interest for practical purposes, as mentioned.

III. ELECTRIC CURRENT DEPENDENCE OF SWITCHING PROBABILITY

In this section, we evaluate the switching probability and investigate the role of the fieldlike torque.

A. Numerically evaluated switching probabilities

Figures 2(a) and 2(b) show two examples of the magnetization dynamics in time domain with the same current density ($j/j_c = 2.0$) and different random field, where $\beta = 0$. The corresponding dynamical trajectories are also shown in Figs. 2(c) and 2(d). The origin of the time, $t = 0$, is set being the time the electric current is injected, i.e., the electric current density is nonzero during $0 \leqslant t \leqslant 5$ ns. The dynamical trajectory shows a curved line in the xz plane as a result of the competition between torques in the LLG equation. For example, the SOT moves the magnetization to the $-y$ direction, however, the precessional torque due to the perpendicular magnetic anisotropy field causes the rotation of the magnetization around the z axis. Accordingly, the magnetization does not directly move to the $-y$ direction; instead, it also moves to the x direction. The magnetization finally saturates to a point at which all torques are balanced; see Eq. (8) in Sec. III B below. The magnetization in Fig. 2(a) succeeds in switching, while that in Fig. 2(b) fails the switching. In particular, the magnetization in Fig. 2(b) firstly shows a precession around the x axis and returns to the positive m_z region after turning off the electric current. Then, the magnetization shows the precessional dynamics near the z axis and relaxes to the initial state $\mathbf{m}_{s+}$. The behavior is similar to the back switching [29] (see also Appendix B). We should, however, recall that the back switching does not appear for this current strength when the temperature is zero, as mentioned at the end of Sec. II B. Therefore, the thermal fluctuation plays a role causing the back switching and leading to the switching error in Fig. 2(b).

Figure 3(a) summarizes the dependence of the switching probability on the electric current density j for $\beta = 0$. Note that the switching probability above $j/j_c \gtrsim 1.0$ decreases as the electric current density increases. This is in contrast to the STT driven magnetization switching, where the switching

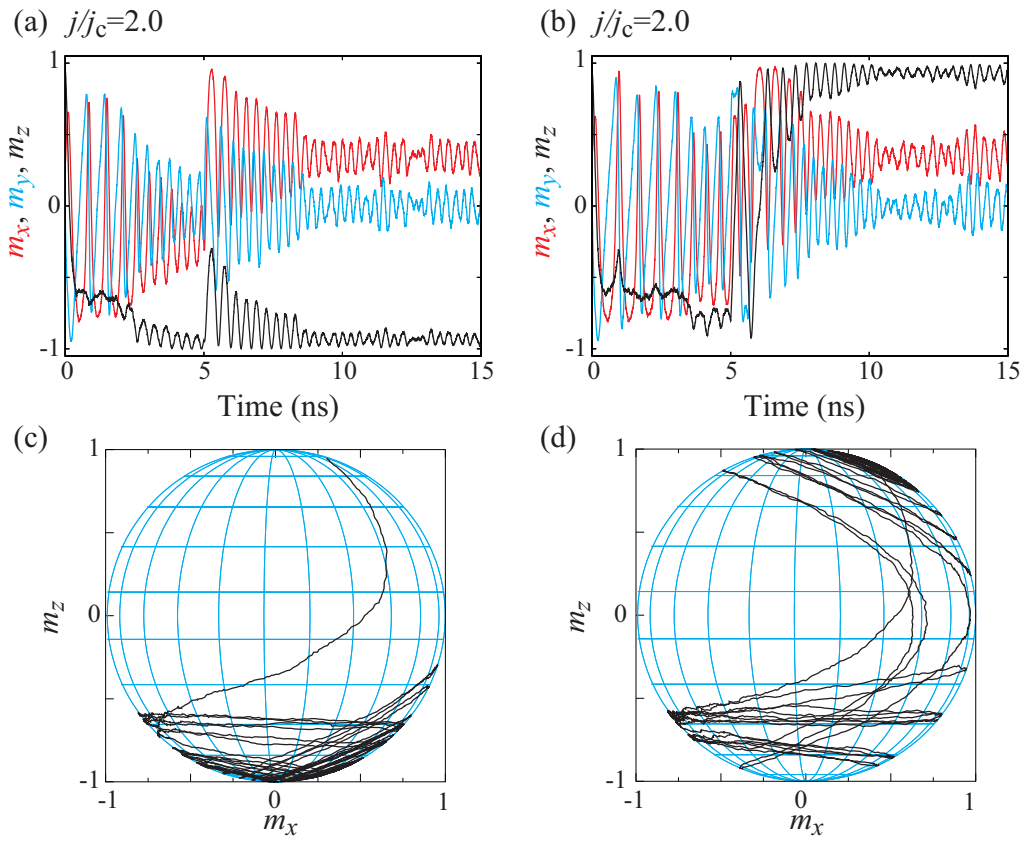

FIG. 2. Examples of the magnetization dynamics in time domain at finite temperature. Current density is common ($j/j_c = 2.0$), however, the random numbers used in the thermal fluctuation are different between (a) and (b). Pulse width of the current is 5 ns, and $\beta = 0$. The magnetization successfully switches its direction after turning off the current in (a), while it is failed in (b). The corresponding dynamical trajectories are shown in (c) and (d).

probability increases monotonically as the electric current density increases [50]. We also evaluate the current dependence of the switching probability for various values of the fieldlike torque, β, as shown in Fig. 3(b). The values of β in Fig. 3(b) were chosen, according to a steady state solution of the LLG equation discussed Sec. III C below. The results indicate that an appropriate value of β ($\beta = -0.50$ in this case) contributes to keep the switching probability high even in the large current regime. This is the main result in this work. In the following, we investigate the interpretations of these results.

B. Switching probability for $\beta = 0$

First, let us investigate on the origin of the decrease of the switching probability in the large current region. This tendency is common for both $\beta = 0$ and $\beta \neq 0$, however, its rate depends on the value of β. In this subsection, we focus on the case of $\beta = 0$. The analysis here will be used to clarify the role of the fieldlike torque in Sec. III C.

It is helpful to briefly review the origin of the back switching [29–31] (see also Appendix B) to distinguish the deterministic and probabilistic natures of the results shown in Fig. 2. For this purpose, we introduce the energy density E, which relates to the magnetic field $\mathbf{H}$ via $\mathbf{H} = -\partial E/\partial(M\mathbf{m})$ and is given by

$$E = -MH_{\rm appl}m_x - \frac{MH_{\rm K}}{2}m_z^2. \tag{7}$$

As mentioned, Eq. (7) has two stable (minimum energy) states, $\mathbf{m}_{s\pm} = (\sin\theta_s, 0, \pm\cos\theta_s)$. In addition, Eq. (7) has one saddle point, $\mathbf{m}_d = +\mathbf{e}_x$, and one unstable (maximum energy) state, $\mathbf{m}_u = -\mathbf{e}_x$. We denote the corresponding energies as $E_s = E(\mathbf{m} = \mathbf{m}_{s\pm}) = -(MH_K/2)[1 + (H_{\rm appl}/H_K)^2]$, $E_d = E(\mathbf{m} = \mathbf{m}_d) = -MH_{\rm appl}$, and $E_u = E(\mathbf{m} = \mathbf{m}_u) = MH_{\rm appl}$. Recall that the torque due to the magnetic field, $-\gamma\mathbf{m} \times \mathbf{H}$, in Eq. (1) induces a precessional dynamic of the magnetization on a constant energy line, i.e., E is kept being constant on a precession trajectory. The damping torque, on the other hand, causes the relaxation dynamics crossing the constant energy lines from higher to lower states. The constant energy line (or the precession trajectory) in the present system is classified into two groups, satisfying $E_s < E < E_d$ and $E_d < E < E_u$; see Fig. 4, where the stable region $S_{+(-)}$ includes the constant energy line in the range of $E_s < E < E_d$ and $\mathbf{m}_{s+(-)}$ while the unstable region U includes the constant energy line in the range of $E_d < E < E_u$ [29]. They are separated by the line $E = E_d$ including the saddle point (the red line in Fig. 4). In Fig. 4, we also show the schematic illustration of the precessional and relaxation dynamics of the magnetization in each region, $S_\pm$ or U, where the black arrows represent the

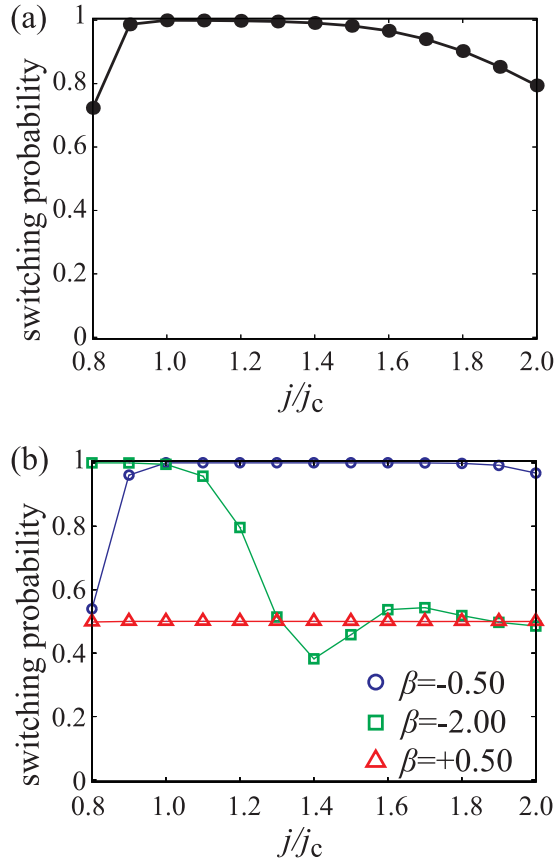

FIG. 3. Switching probability for 10^7 trials as a function of the electric current density j with respect to the critical value j_c. The value of β is zero in (a) while that is varied as $\beta = -0.50$ (blue circles), -2.0 (green squares), and $+2.0$ (red triangles) in (b).

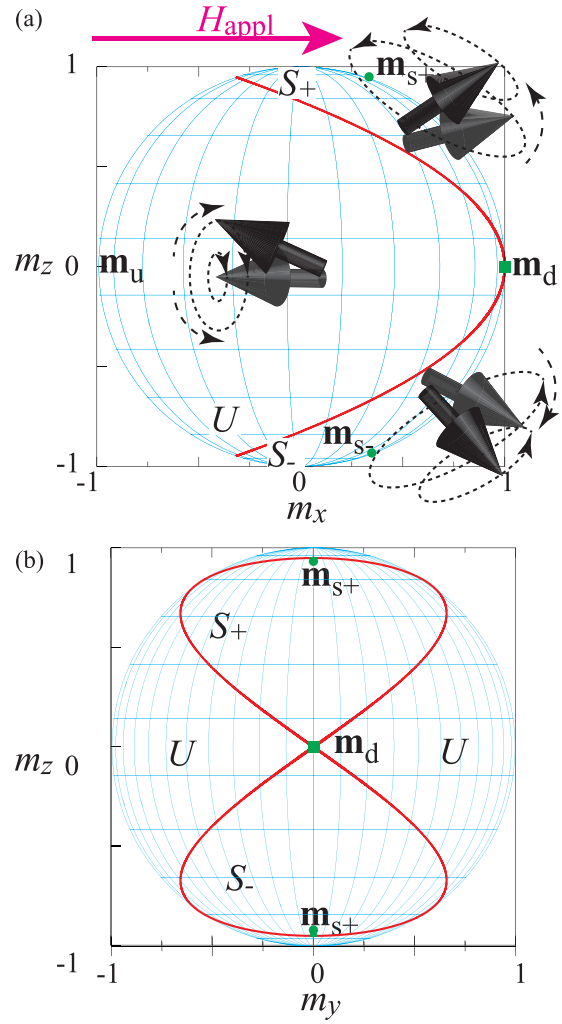

FIG. 4. Schematic illustration of the energetically stable and unstable regions, $S_\pm$ and U, in (a) xz and (b) yz planes. The directions of the stable states (minimum energy states) are denoted as $\mathbf{m}_{s\pm}$, while the saddle point and unstable state (maximum energy state) are represented as $\mathbf{m}_d$, and $\mathbf{m}_u$, respectively. The black arrows schematically show the precessional and relaxation dynamics of the magnetization in each region, where the short dashed circular and long dashed lines represent the precessional and relaxation directions. The red line represents a constant energy curve including the saddle point, indicating the boundaries between $S_\pm$ and U. Green dots and squares represent the positions of $\mathbf{m}_{s\pm}$ and $\mathbf{m}_d$, respectively.

magnetization while the short dashed circular and long dashed lines represent the precession and relaxation directions, respectively.

By applying the electric current density, SOT brings the magnetization to a steady state. When this state locates in the stable region $S_\pm$, the magnetization relaxes to the nearest stable state $\mathbf{m}_{s\pm}$ after turning off the current. When the steady state in the presence of the current is inside the unstable region U, on the other hand, the magnetization starts to precess around the x axis due to the precessional torque and moves to the boundaries between the stable (S_+ or S_-) and unstable (U) regions due to the damping torque. When the magnetization crosses the boundary between $S_{+(-)}$ and U, it relaxes to the stable state $\mathbf{m}_{s+(-)}$. Which of two boundaries the magnetization crosses depends on several parameters, such as the electric current density and the damping constant. When the magnetization crosses the boundary between the stable state of the initial state (S_+ in the present work) and the unstable state U, the magnetization returns to the initial state; this is the back switching. Accordingly, the back switching has the deterministic nature.

When the electric current density satisfies $j/j_{th} < 1$, the magnetization at zero temperature finally saturates to the region S_- by the SOT, and thus, the back switching does not occur. However, in the presence of the thermal fluctuation at finite temperature, the magnetization enters the region U probabilistically during the application of the electric current density or even after turning off the current. The magnetization in Fig. 2(a) safely stays inside the region S_- and relaxes to the switched state, while it in Fig. 2(b) enters the region U and the back switching occurs. The rate whether the magnetization probabilistically enters the region U increases as the electric current density increases due to the following reason. A steady state solution of the LLG equation satisfying $m_z < 0$ is given by (see also Appendix C)

$$\cos\theta = -\frac{H_{appl}}{H_s}, \quad \cos\varphi = -\frac{H_{appl}H_K}{H_s\sqrt{H_s^2 - H_{appl}^2}}, \tag{8}$$

where the zenith and azimuth angles (θ and φ) satisfy $\mathbf{m} = (m_x, m_y, m_z) = (\sin\theta\cos\varphi, \sin\theta\sin\varphi, \cos\theta)$. We also assume that $s > h$, which is satisfied for $j/j_c \gtrsim 1.2$ for the present parameter. These solutions indicate that the steady state saturates to the y direction in the large current limit. It means that the steady state becomes close to, or even enters, the unstable region U as the electric current density increases. Then, the probability that the magnetization enters the region U also increases. This is the origin of the reduction of the switching probability due to the back switching in the large current region shown in Fig. 3(a).

C. Switching probability for $\beta \neq 0$

Now let us investigate the effect of the fieldlike torque on the switching probability. The main result in Fig. 3(b) is that the switching probability is kept being high even in the large current region when an appropriate fieldlike torque ($\beta = -0.50$ in this case) is introduced. In other words, the switching probability compared to the case of $\beta = 0$ is recovered by the fieldlike torque. We notice that this recovery comes from an effective enhancement of the damping torque by introducing the fieldlike troque. We explain this argument in the following.

Let us firstly focus on the SOT strength in the case of $\beta = 0$. Figures 5(a) and 5(b) show the numerically obtained and the schematic illustration of the projection of the precession trajectory of the magnetization to the xy plane, where the time range is $t \leqslant 5$ ns, i.e., we show the trajectory in the presence of the SOT. In Fig. 5(a), the red circle represents the initial state, and the temperature is set to be zero to show the trajectory clearly. The precessional torque due to the perpendicular magnetic anistoropy field causes a circular rotation of the magnetization in the xy plane. Because of the applied magnetic field in the x direction, however, the trajectory becomes asymmetric with respect to the y axis. For the following discussion, we should note that the damping torque points to the stable point ($\mathbf{m}_{s-}$), which locates near the center of the xy plane. The arrows in Fig. 5(b) indicate the (dampinglike) SOT direction on the trajectory. Recall that the SOT for the present case moves the magnetization to the negative y direction. Therefore, when the magnetization direction locates at $m_x = 0$, the SOT points orthogonal to the damping torque, as schematically shown as "SOT⊥ DT" in Fig. 5(b) (we denote the damping torque as "DT" in Figs. 5(a) and 5(b), for simplicity). In this case, the SOT does not enhance nor reduce the damping torque. When the magnetization shifts from $m_x = 0$, however, the SOT has a projection to the direction of the damping torque. For example, the SOT becomes approximately parallel to the damping torque when $m_y > 0$ while that becomes approximately antiparallel to the damping torque when $m_y < 0$, as schematically shown in Fig. 5(a) as "SOT∥ +DT" and "SOT∥ −DT". It should be emphasized that the average of the SOT is zero, the SOT does not enhance nor reduce the damping torque in this case. This is because the SOT strength depends on the relative angle between the magnetization and the y axis, and because of the axial symmetry of the precessional trajectory along the x axis, the SOTs for $m_y > 0$ and $m_y < 0$ have the same magnitude but the opposite sign.

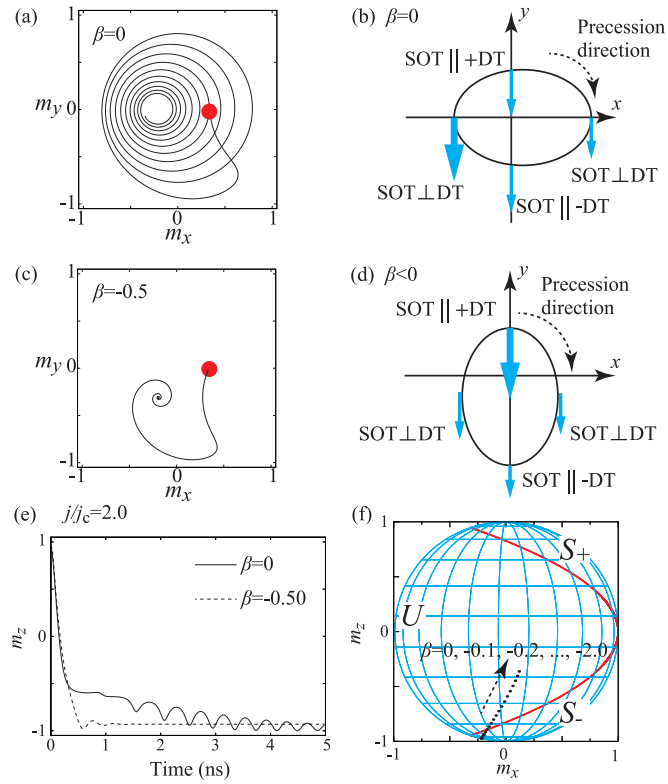

FIG. 5. (a) Numerically obtained and (b) schematic illustration of the projection of the precession trajectory to the xy plane for $\beta = 0$. The blue arrows in (b) indicate the projection of the dampinglike SOT at each point on the dynamic trajectory in the xy plane. Damping torque is denoted as "DT", for simplicity. The magnitude of the arrow schematically illustrates its strength. Recall that SOT strength is large when the relative angle between the magnetization and the y axis is close to 90°. Thus, the SOT strength when the magnetization comes at a point $m_x = 0$ and $m_y > 0$ is the same to that when the magnetization comes to another point $m_x = 0$ and $m_y < 0$ at a different time; however, while the former has a projection to the direction parallel to the damping torque, the latter has a projection antiparallel to it. As a result, their average becomes zero. (c) Numerically obtained and (d) schematic illustration of the projection of the precession trajectory to the xy plane for $\beta < 0$. The shape change of the trajectory to the x direction due to the applied magnetic field is neglected in (d), for simplicity, to show the change of the precession trajectory by the fieldlike torque clearly. In this case, the dampinglike SOT parallel to the damping torque is stronger than that antiparallel to the damping torque. As a result, the averaged SOT has a finite contribution to the damping torque. (e) Examples of time evolution of m_z at zero temperature for $\beta = 0$ (solid line) and $\beta = -0.50$ (dotted line). (f) Steady state solution of the magnetization for various negative fieldlike torque ($\propto \beta$) shown on a unit sphere. The electric current density is $j/j_c = 2.0$. The red line represents a constant energy curve including the saddle point, indicating the boundaries between $S_\pm$ and U. In (c) and (d), the temperature is zero to show the role of the fieldlike torque clearly.

The introduction of the fieldlike torque changes this situation. The fieldlike torque acts as a torque due to an applied magnetic field pointing the y direction and changes the precession trajectory. Figures 5(c) and 5(d) show the numerically

obtained and the schematic illustration of the precession trajectory in the presence of negative ($\beta < 0$) fieldlike torque. The trajectory is extended to the negative y direction in this case; in Fig. 5(d), we neglect the applied magnetic field in the x direction for simplicity to show the modulation of the precession trajectory by the fieldlike torque clearly. Due to this asymmetric trajectory, the strengths of the dampinglike SOT for $m_y > 0$ and $m_y < 0$ are different. As a result, the averaged dampinglike SOT has a finite contribution to the damping torque. In particular, when β is negative, the dampinglike SOT parallel to the damping torque is larger than that antiparallel to the damping torque, as shown in Fig. 5(b). As a result, the averaged dampinglike SOT effectively enhances the damping torque.

These schematic considerations can be confirmed by analyzing the temporal dynamics shown in Fig. 5(e), where m_z for $\beta = 0$ (solid line) and $\beta = -0.50$ (dotted line) are shown. The temperature is set to be zero, for simplicity, to reveal the role of the fieldlike torque clearly. As shown, m_z immediately relaxes to the steady state when β is finite. On the other hand, when $\beta = 0$, m_z shows a small-amplitude oscillation before saturating to the steady state, which corresponds to an oscillating motion of the magnetization near the boundary between the regions of S_- and U (see also Appendix B, where the dynamical trajectory on the unit sphere is shown). These results are consistent with the above interpretation that the introduction of the fieldlike torque leads to an effective modulation of the damping torque. When $\beta = 0$ and at finite temperature, the magnetization probabilistically enters the unstable region due to the oscillation occurring near the boundary between the regions S_- and U. As a result, the back switching possibly occurs, and the switching probability becomes small. For $\beta < 0$, on the other hand, the magnetization immediately relaxes to the steady state, which locates inside the region S_-, and the back switching can be avoided. Therefore, the switching probability is kept being high for the case of $\beta = -0.50$ in Fig. 3(b).

Figure 3(b) also indicates that the value of β should be appropriately chosen to keep the high switching probability. For positive β, it was already shown in Ref. [43] that the magnetization direction is approximately fixed to the xy plane and hardly reaches to the negative m_z region. This is because the SOT effectively acts as an antidamping torque when the magnetization enters the negative m_z region and tries to keep the magnetization to the xy plane. Therefore, the switching probability is approximately 50% for the positive β. For negative and sufficiently large β, the switching probability decreases as the electric current density increases. This is because a large fieldlike torque brings the steady state of the magnetization to the y direction, which locates inside the unstable region U; therefore, the back switching possibly occurs. This point can be confirmed by evaluating the dependence of the steady state on the magnitude of β, as shown in Fig. 5(f). Although we could not obtain an analytical solution of the steady state for a nonzero β, the numerical result indicates that the magnetization enters the unstable region U when $\beta \lesssim -0.7$. Therefore, the back switching possibly occurs for a large negative β, and the switching probability becomes small in the large current limit, as shown in Fig. 3(b). The values of β (-0.5 and -2.0) were chosen so that the steady state solution enters the stable or unstable region and the back switching possibly occurs or not.

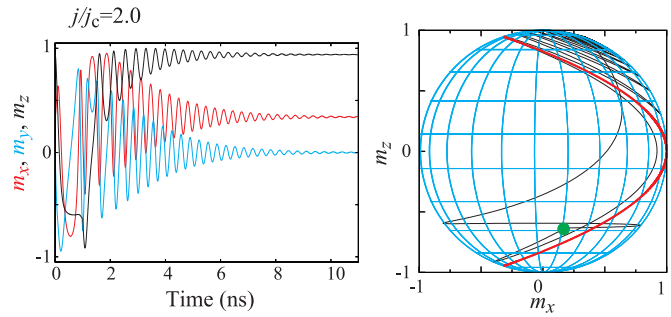

FIG. 6. An example of the magnetization dynamics in time domain (left) and on a unit sphere (right) at zero temperature. Current density is $j/j_c = 2.0$, temperature is zero, and $\beta = 0$. The pulse width is 1 ns. Green dot in the right figure indicates the magnetization direction when the electric current density is turned off. The red line indicates the constant energy curve of $E = E_d$.

Regarding the above result, the fieldlike torque may provide a solution to achieve the reliable switching (another solution may be using a large damping material; see Appendix D). We, however, note that the values of the parameters are appropriately chosen. In fact, the switching probability even for $\beta = -0.50$ shows a decrease as the electric current density increases, as shown in Fig. 3(b). This is because the steady state of the magnetization moves to the y direction ($\in U$) when the electric current density is sufficiently large. Therefore, the back switching in the sufficiently large current region is unavoidable even in the presence of the fieldlike torque. Note also that whether the magnetization in the steady state locates in the stable or unstable region is independent of the damping parameter α because the steady state solution is obtained by the condition $d\mathbf{m}/dt = \mathbf{0}$; therefore, the condition $\beta \lesssim -0.7$ mentioned above, for example, is unchanged even when the value of α is changed. A large α, however, leads to a fast relaxation of the magnetization (see Appendix D) and may contribute to keep the high switching probability even for a negatively large β. Summarizing them, appropriate control of the system parameters will be required for practical applications.

IV. SWITCHING PROBABILITY FOR SHORT CURRENT PULSE

Here, we recalculate the magnetization dynamics at zero and finite temperature by changing the pulse width t_p to 1 ns and compare the results with those shown in Sec. III.

An important difference between the long and short current pulse is that the magnetization in the latter case does not reach the steady state when the electric current density is turned off. An example is shown in Fig. 6, where the magnetization dynamics for $j/j_c = 2.0$ and $\beta = 0$ is shown. The temperature is assumed to be zero to clearly show the magnetization direction when the electric current density is turned off. We notice that the magnetization at $t = t_p$, shown by the green circle in the bottom figure of Fig. 6, locates in the unstable region U. Recall that the steady state solution ($t \to \infty$) for this case locates in the stable region S_- because

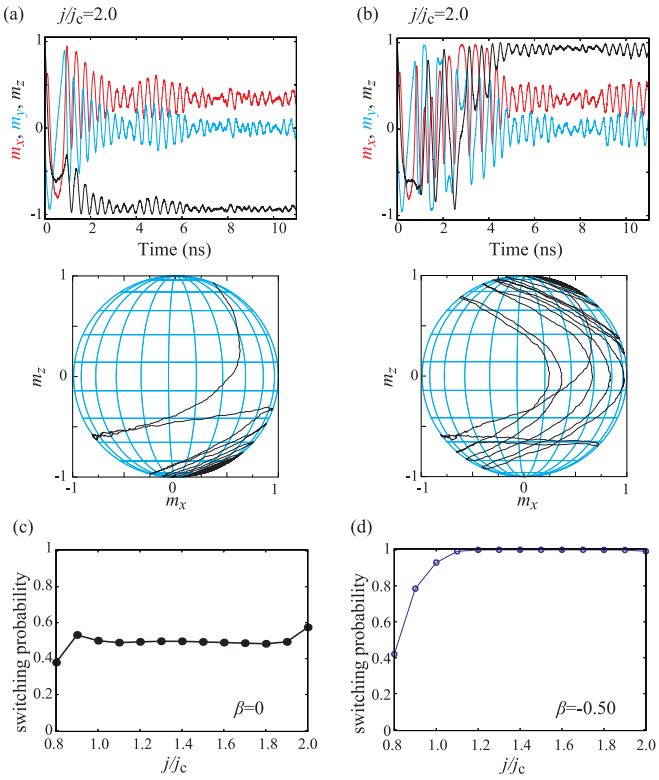

FIG. 7. Examples of the magnetization dynamics in time domain (top) and on a unit sphere (bottom) at finite temperature. Current density is common ($j/j_c = 2.0$), however, the random numbers used in the thermal fluctuation are different between (a) and (b). Pulse width of the current is 1 ns, and $\beta = 0$. The magnetization successfully switches its direction after turning off the current in (a), while it is failed in (b). Current dependences of the switching probability for $\beta = 0$ and $\beta = -0.50$ are shown in (c) and (d), respectively.

the condition $j/j_{\rm th} < 1$ is satisfied. However, since the pulse width is short, the magnetization cannot reach the steady state in the case of Fig. 6. Accordingly, after turning off the current, the magnetization starts to precess around the x axis and the back switching occurs. As can be seen in this example, the back switching possibly occurs even at zero temperature when the pulse width is short. Therefore, the switching probability is expected to be small compared to the long pulse-width case.

Figures 7(a) and 7(b) show the examples of the magnetization dynamics at finite temperature ($T = 300$ K). In the case of Fig. 7(a), the thermal fluctuation assists the magnetization to enter the region S_-, and thus, the switching is achieved even though the pulse width of the current is short. In the case of Fig. 7(b), on the other hand, the back switching occurs, and the magnetization fails the switching. Figure 7(c) summarizes the dependence of the switching probability on the current for $\beta = 0$. Compared to Fig. 3(a), the switching probability is significantly suppressed and stays near 50%. This is because the back switching possibly occurs due to the short pulse width, and thus, whether the switching occurs or not sensitively depends not only on the thermal fluctuation but also on the system parameters. We notice that this issue is again solved by an appropriate fieldlike torque. Figure 7(d) shows the current dependence of the switching probability, where $\beta = -0.50$. The switching probability is kept being high for a wide range of the current. This is because the presence of the fieldlike torque leads to the fast relaxation of the magnetization to the steady state, as can be seen in Fig. 5(d), and thus, the magnetization immediately reach the stable region S_- even when the pulse width is short.

V. CONCLUSION

In summary, the probability of the SOT driven magnetization switching is evaluated by numerical simulation of the LLG equation, where the ferromagnet is perpendicularly magnetized and an in-plane magnetic field is applied. The switching probability in the large current region decreases as the current magnitude increases. This is due to the combination of the back switching and the thermal fluctuation, which have deterministic and probabilistic natures, respectively. The result is in contrast to the conventional STT switching, where the switching probability increases monotonically. It is found that the fieldlike torque with an appropriate value suppresses the switching error due to the back switching and contributes to recover the high switching probability. This is because the introduction of such a fieldlike torque leads to an effective enhancement of the damping torque and contributes to achieving the fast relaxation to the switched state, which is clarified from the temporal analysis of the magnetization dynamics.

ACKNOWLEDGMENTS

This work was supported by funding from the TDK Corporation. The author is grateful to Shinji Isogami, Shuji Okame, Katsuyuki Nakada, Tomoyuki Sasaki, Seiji Mitani, and Masamitsu Hayashi for valuable discussion.

DATA AVAILABILITY

The data that support the findings of this article are not publicly available because they contain commercially sensitive information. The data are available from the authors upon reasonable request.

APPENDIX A: NUMERICAL METHOD TO SOLVE THE LLG EQUATION

We apply the fourth order Runge-Kutta method to solve the LLG equation; however, accuracy may be the second order due to the following reason. We express the LLG equation as $d\mathbf{m}/dt = \mathbf{T}(t)$, for simplicity, and the magnetization $\mathbf{m}$ at time $t_n = t_0 + n\Delta t$ as $\mathbf{m}_n = \mathbf{m}(t_0 + n\Delta t)$, where t_0 is the initial time and $\Delta t = 1$ ps is the infinitesimally short time increment. The right-hand side of Eq. (1) is denoted as $\mathbf{T}(t)$, for simplicity. The time development of $\mathbf{m}$ from $\mathbf{m}_n$ to $\mathbf{m}_{n+1}$ is given by

$$\mathbf{m}_{n+1} = \mathbf{m}_n + \tfrac{1}{6}(\mathbf{k}_1 + 2\mathbf{k}_2 + 2\mathbf{k}_2 + \mathbf{k}_4), \qquad \text{(A1)}$$

where $\mathbf{k}_i$ $(i = 1, 2, 3, 4)$ are defined as $\mathbf{k}_1 = \Delta t\mathbf{T}(t_n, \mathbf{X}_{n,1})$, $\mathbf{k}_2 = \Delta t\mathbf{T}(t_n + \Delta t/2, \mathbf{X}_{n,2})$, $\mathbf{k}_3 = \Delta t\mathbf{T}(t_n + \Delta t/2, \mathbf{X}_{n,3})$, and $\mathbf{k}_4 = \Delta t\mathbf{T}(t_n + \Delta t, \mathbf{X}_{n,4})$ with $\mathbf{X}_{n,1} = \mathbf{m}_n$, $\mathbf{X}_{n,2} = \mathbf{m}_n + \mathbf{k}_1/2$, $\mathbf{X}_{n,3} = \mathbf{m}_n + \mathbf{k}_2/2$, and $\mathbf{X}_{n,4} = \mathbf{m}_n + \mathbf{k}_3$. The

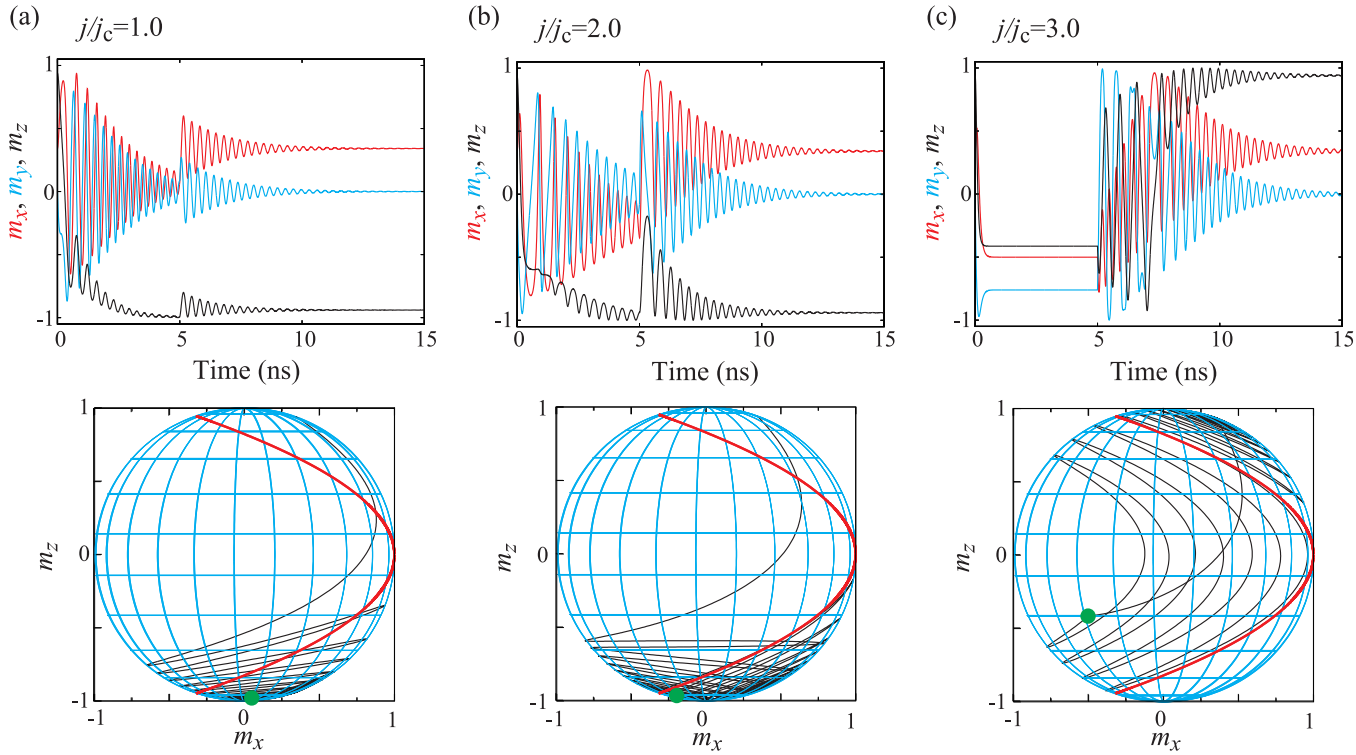

FIG. 8. Examples of magnetization dynamics in time domain (top) and on a unit sphere (bottom) for j/j_c of (a) 1.0, (b) 2.0, and (c) 3.0. Temperature is zero, and pulse width of the electric current is 5 ns. In the bottom figure, green dots schematically represent the magnetization direction when the electric current density is turned off, while red lines indicate constant energy lines including the saddle point; see Fig. 3(a).

Mersenne Twister [51] was used to generate random numbers, and the Box-Muller transformation was adopted to transform the distribution of the random number from the uniformly to the standard normal one. In our calculation, however, we assume that the random field $\mathbf{h}(t)$ is constant during Δt and use the same value for $\mathbf{T}(t_n, \mathbf{X}_{n,1})$, $\mathbf{T}(t_n + \Delta t/2, \mathbf{X}_{n,2})$, $\mathbf{T}(t_n + \Delta t/2, \mathbf{X}_{n,3})$, and $\mathbf{T}(t_n + \Delta t, \mathbf{X}_{n,4})$. Using such a simplification may lower the accuracy of the calculations to the second order, while there have been some proposals to perform the higher-order Runge-Kutta method with random variables [52,53]. However, the complexity in algorithms further increases. In addition, these methods require a large number of random variables, and generating random numbers costs huge calculation time.

APPENDIX B: CRITICAL AND THRESHOLD CURRENT DENSITIES AND BACK SWITCHING

Here, we show some examples of the back switching and review its origin in detail. Let us focus on a perpendicularly magnetized ferromagnet, which has two energetically stable states. Although the back switching occurs not only in a perpendicular ferromagnet [29] but also in an in-plane magnetized ferromagnet [30,31], we focus on the perpendicularly magnetized ferromagnet here, as in the case of the main text. For convenience, we assume that the magnetization initially points to the positive z direction. When the electric current density is applied to the nonmagnetic electrode, the SOT moves the magnetization to the negative m_z region. However, depending on the parameters, the magnetization returns to the initial state after turning off the electric current density. The phenomenon occurs even when the thermal fluctuation is absent; thus, the back switching is deterministic dynamics. It was found in Ref. [28] and its origin was investigated in Ref. [29]. It was pointed out in Ref. [30] that the same phenomenon occurs in SOT devices with an in-plane magnetized ferromagnetic free layer, and the phenomenon was named as the back switching in Ref. [31] to distinguish it with the back hopping in STT devices [54,55].

Figures 8(a)–8(c) show examples of the magnetization dynamics in time domain (top) and on the unit sphere (bottom). The electric current densities with respect to j_c are (a) 1.0, (b) 2.0, and (c) 3.0, while the temperature is zero. In the bottom figures, the magnetization direction when the electric current density is turned off is indicated by the solid green circle. In addition, the constant energy curve of $E = E_d$ is indicated by the red solid line. The pulse width of the current is 5 ns. Recall that $j_{th}/j_c \simeq 2.3$; therefore, when the electric current density satisfies $j/j_{th} \lesssim 2.3$, the steady state of the magnetization locates in the stable region S_-. This argument can be confirmed from Figs. 8(a) and 8(b). In this case, the back switching does not occur at zero temperature. On the other hand, the steady state of the magnetization locates in the unstable region U when $j/j_c = 5.0$; see Fig. 8(c). In this case, the magnetization starts to precess around the x axis after turning off the electric current density, and the back switching occurs. Note that whether the back switching occurs or not depends on the values of the parameters; thus, even when the electric current density is larger than j_{th}, the magnetization switching may be achieved. It is also confirmed that the magnetization (and m_z) oscillates around the boundary (red

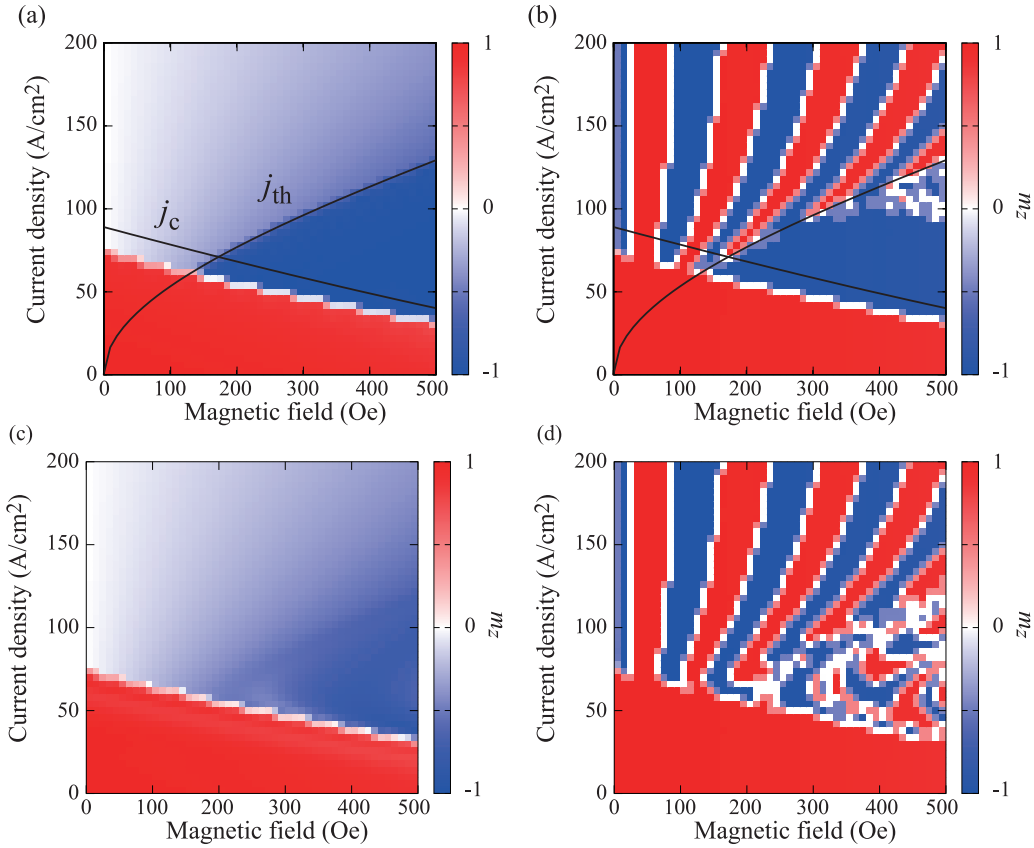

FIG. 9. Phase diagram of m_z (a) when the electric current density is turned off and (b) 10 ns after turning off the current. The pulse width of the electric current density is 5 ns, temperature is zero, and $\beta = 0$. Those for the pulse width of 1 ns are shown in (c) and (d), respectively. In (a) and (b), j_c and j_{th} are also shown by solid lines.

line) between the regions S_- and U, as mentioned in Sec. III C.

Figures 9(a) and 9(b) summarize the value of m_z, where the former shows m_z in the steady state in the presence of the SOT while the latter shows the relaxed value of m_z after turning off the current. The values of j_c and j_{th} estimated from Eqs. (5) and (6) are also shown by the solid lines. It can be confirmed that the magnetization switches its direction for the current range of $j_c < j < j_{th}$. On the other hand, for $j > j_{th}$, the region where $m_z = +1$ and $m_z = -1$ appears alternately in Fig. 9(b), which corresponds to the back switching region [31]. Note that Eq. (6) provides a well estimation of the boundary between the switched and back switching regions. There is, on the other hand, a slight different between Eq. (5) and the boundary between the non-switched and switched or back switching regions. This difference comes from an assumption used in Ref. [28] to derive Eq. (5). Reference [28] assumes a finite rising time of the electric current density. In this case, the SOT initially contributes to move the magnetization from the z axis slightly. After that, however, the magnetization dynamics to the negative z direction is mainly caused by the precessional torque due to the in-plane magnetic field along the x axis until the current magnitude is saturated. Then, the magnetization dynamics is restricted in a region satisfying $m_y = 0$ for a while, as shown by the numerical simulation in Ref. [28]. This fact makes it easy to solve the steady state LLG equation analytically and enables to derive the analytical formula given by Eq. (5). The dependence of the switching behavior on the rise time and the effect of the field-like torque on it is studied in Ref. [42]. However, an accurate illustration of the current pulse shape requires circuit analyses, which is beyond the scope of this paper. For simplicity, in this work, we assume the step-function-like injection of the electric current density. We also note that a formula similar to Eq. (5) was also derived in Ref. [56] for a different purpose.

As mentioned in Sec. IV, the magnetization cannot reach the steady state in the presence of SOT when the pulse width of the electric current density is short. Figures 9(c) and 9(d) show m_z for the pulse width of 1 ns. Comparing Fig. 9(c) to Fig. 9(a), it is found that m_z in the current range of $j_c < j < j_{th}$ strongly depends on the pulse width. As a result, the back switching possibly occurs even in this current range, as can be seen in Fig. 9(d).

APPENDIX C: STEADY STATE SOLUTION OF MAGNETIZATION

Equation (8) is derived from the LLG equation in terms of the zenith and azimuth angles, θ and φ. In the steady state ($d\mathbf{m}/dt = \mathbf{0}$), the LLG equation becomes

$$H_{\rm appl} \sin\varphi + H_{\rm s} \cos\theta \sin\varphi = 0, \tag{C1}$$

$$H_{\rm K} \sin\theta \cos\theta - H_{\rm appl} \cos\theta \cos\varphi - H_{\rm s} \cos\varphi = 0. \tag{C2}$$

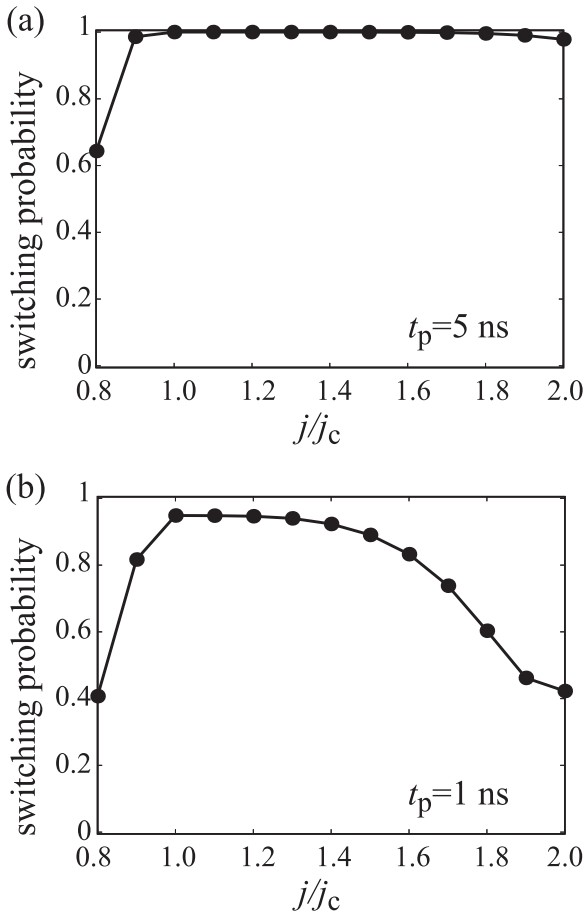

FIG. 10. Current dependence of the switching probability for the large damping material ($\alpha = 0.10$). The pulse width of the current is (a) 5 and (b) 1 ns.

Here, the fieldlike torque is neglected. For the present convention ($H_{appl}/H_K > 0$ and $H_s/H_K > 0$), the steady state for $j/j_c \gg 1.0$ locates at $m_y, m_z < 0$ while $\sin\theta > 0$ because of its definition ($0 \leqslant \theta \leqslant \pi$). Using these facts, the steady state solution of θ and φ are given by Eq. (8).

APPENDIX D: SWITCHING PROBABILITY OF LARGE DAMPING MATERIAL

It is shown in the main text that the fieldlike torque contributes to keep the switching probability in the large current region high. Another solution is using large damping materials as the ferromagnetic free layer because of the following reason. As mentioned in the main text, the back switching originates from the precession of the magnetization around the x axis after turning off the current. However, when the damping constant is large, the magnetization immediately relaxes to the nearest stable state without precessing around the x axis many times. Therefore, the back switching can be avoided. In fact, the previous works focused on the large damping materials [28,49], where the back switching was not discussed.

We investigate that the large damping materials lead to the reliable switching even in the large current region. Figures 10(a) and 10(b) summarize the current dependences of the switching probability for the pulse widths of 5 and 1 ns, respectively. The damping constant is $\alpha = 0.10$. Comparing Fig. 10(a) to Fig. 3(a), it is confirmed that using the large damping materials results in keeping the switching probability high even in the large current region. Even for the short current pulse, the switching probability becomes relatively high due to the large damping materials, although the switching probability in the large current region becomes small; see Figs. 7(c) and 10(b). Therefore, using the large damping materials may be another solution to keep the high switching probability. We, however, note that the value of $\alpha = 0.10$ is relatively large compared to that found in typical ferromagnets used in SOT devices, such as Fe, Co, and Ni, and their alloys [57]. There may be some ferromagnetic materials having such a large α; however, such materials should also show high magnetoresistance effect for practice.

[1] L. Liu, C.-F. Pai, Y. Li, H. W. Tseng, D. C. Ralph, and R. A. Buhrman, Spin-torque switching with the giant spin Hall effect of tantalum, Science **336**, 555 (2012).
[2] L. Liu, O. J. Lee, T. J. Gudmundsen, D. C. Ralph, and R. A. Buhrman, Current-induced switching of perpendicularly magnetized magnetic layers using spin torque from the spin Hall effect, Phys. Rev. Lett. **109**, 096602 (2012).
[3] C.-F. Pai, L. Liu, Y. Li, H. W. Tseng, D. C. Ralph, and R. A. Buhrman, Spin transfer torque devices utilizing the giant spin Hall effect of tungsten, Appl. Phys. Lett. **101**, 122404 (2012).
[4] M. I. Dyakonov and V. I. Perel, Current-induced spin orientation of electrons in semiconductors, Phys. Lett. A **35**, 459 (1971).
[5] J. E. Hirsch, Spin Hall effect, Phys. Rev. Lett. **83**, 1834 (1999).
[6] S. Zhang, Spin Hall effect in the presence of spin diffusion, Phys. Rev. Lett. **85**, 393 (2000).
[7] J. C. Slonczewski, Current-driven excitation of magnetic multilayers, J. Magn. Magn. Mater. **159**, L1 (1996).
[8] L. Berger, Emission of spin waves by a magnetic multilayer traversed by a current, Phys. Rev. B **54**, 9353 (1996).
[9] J. A. Katine, F. J. Albert, R. A. Buhrman, E. B. Myers, and D. C. Ralph, Current-driven magnetization reversal and spin-wave excitations in Co/Cu/Co pillars, Phys. Rev. Lett. **84**, 3149 (2000).
[10] E. B. Myers, F. J. Albert, J. C. Sankey, E. Bonet, R. A. Buhrman, and D. C. Ralph, Thermally activated magnetic reversal induced by a spin-polarized current, Phys. Rev. Lett. **89**, 196801 (2002).
[11] S. I. Kiselev, J. C. Sankey, I. N. Krivorotov, N. C. Emley, R. J. Schoelkopf, R. A. Buhrman, and D. C. Ralph, Microwave oscillations of a nanomagnet driven by a spin-polarized current, Nature (London) **425**, 380 (2003).
[12] H. Kubota, A. Fukushima, Y. Ootani, S. Yuasa, K. Ando, H. Maehara, K. Tsunekawa, D. D. Djayaprawira, N. Watanabe, and Y. Suzuki, Evaluation of spin-transfer switching in

CoFeB/MgO/CoFeB magnetic tunnel junctions, Jpn. J. Appl. Phys. **44**, L1237 (2005).

[13] P. M. Braganca, I. N. Krivorotov, O. Ozatay, A. G. F. Garcia, N. C. Emley, J. C. Sankey, D. C. Ralph, and R. A. Buhrman, Reducing the critical current for short-pulse spin-transfer switching of nanomagnets, Appl. Phys. Lett. **87**, 112507 (2005).

[14] I. N. Krivorotov, N. C. Emley, J. C. Sankey, S. I. Kiselev, D. C. Ralph, and R. A. Buhrman, Time-domain measurements of nanomagnet dynamics driven by spin-transfer torques, Science **307**, 228 (2005).

[15] Z. Diao, D. Apalkov, M. Pakala, Y. Ding, A. Panchula, and Y. Huai, Spin transfer switching and spin polarization in magnetic tunnel junctions with MgO and AlO_x barriers, Appl. Phys. Lett. **87**, 232502 (2005).

[16] Edited by B. Dieny, R. B. Goldfarb, and K.-J. Lee, in *Introduction to Magnetic Random-Access Memory* (Wiley-IEEE Press, Hoboken, 2016).

[17] G. Yu, P. Upadhyaya, Y. Fan, J. G. Alzate, W. Jiang, K. L. Wong, S. Takei, S. A. Bender, L.-T. Chang, Y. Jiang, M. Lang, J. Tang, Y. Wang, Y. Tserkovnyak, P. K. Amiri, and K. L. Wang, Switching of a perpendicular magnetization by spin-orbit torques in the absence of external magnetic fields, Nat. Nanotechnol. **9**, 548 (2014).

[18] L. You, O. Lee, D. Bhowmik, D. Labanowski, J. Hong, J. Bokor, and S. Salahuddin, Switching of perpendicularly polarized nanomagnets with spin orbit torque without an external magnetic field by engineering a tilted anisotropy, Proc. Natl. Acad. Sci. USA **112**, 10310 (2015).

[19] J. Torrejon, F. Garcia-Sanchez, T. Taniguchi, J. Sinha, S. Mitani, J.-V. Kim, and M. Hayashi, Current-driven asymmetric magnetization switching in perpendicularly magnetized CoFeB/MgO heterostructures, Phys. Rev. B **91**, 214434 (2015).

[20] S. Fukami, T. Anekawa, C. Zhang, and H. Ohno, Magnetization switching by spin-orbit torque in an antiferromagnet-ferromagnet bilayer system, Nat. Mater. **15**, 535 (2016).

[21] Y.-C. Lau, D. Betto, K. Rode, J. M. D. Coey, and P. Stamenov, Spin-orbit torque switching without an external field using interlayer exchange coupling, Nat. Nanotechnol. **11**, 758 (2016).

[22] M. Wang, W. Cai, D. Zhu, Z. Wang, J. Kan, Z. Zhao, K. Cao, Z. Wang, Y. Zhang, T. Zhang, C. Park, J.-P. Wang, A. Fert, and W. Zhao, Field-free switching of a perpendicular magnetic tunnel junction through the interplay of spin-orbit and spin-transfer torques, Nat. Electron. **1**, 582 (2018).

[23] E. Grimaldi, V. Krizakova, G. Sala, F. Yasin, S. Couet, G. S. Kar, K. Garello, and P. Gambardella, Single-shot dynamics of spin-orbit torque and spin transfer torque switching in three-terminal magnetic tunnel junctions, Nat. Nanotechnol. **15**, 111 (2020).

[24] T. Taniguchi, J. Grollier, and M. D. Stiles, Spin-transfer torques generated by the anomalous Hall effect and anisotropic magnetoresistance, Phys. Rev. Appl. **3**, 044001 (2015).

[25] V. P. Amin and M. D. Stiles, Spin transport at interfaces with spin-orbit coupling: Formalism, Phys. Rev. B **94**, 104419 (2016).

[26] V. P. Amin and M. D. Stiles, Spin transport at interfaces with spin-orbit coupling: Phenomenology, Phys. Rev. B **94**, 104420 (2016).

[27] S.-h. C. Baek, V. P. Amin, Y.-W. Oh, G. Go, S.-J. Lee, G.-H. Lee, K.-J. Kim, M. D. Stiles, B.-G. Park, and K.-J. Lee, Spin currents and spin-orbit torques in ferromagnetic trilayers, Nat. Mater. **17**, 509 (2018).

[28] K.-S. Lee, S.-W. Lee, B.-C. Min, and K.-J. Lee, Theoretical current for switching of a perpendicular magnetic layer induced by spin Hall effect, Appl. Phys. Lett. **102**, 112410 (2013).

[29] T. Taniguchi, Theoretical condition for switching the magnetization in a perpendicularly magnetized ferromagnet via the spin Hall effect, Phys. Rev. B **100**, 174419 (2019).

[30] T. Taniguchi, Switching induced by spin Hall effect in an in-plane magnetized ferromagnet with the easy axis parallel to the current, Phys. Rev. B **102**, 104435 (2020).

[31] T. Taniguchi, Y. Shiokawa, and T. Sasaki, Reduction of back switching by large damping ferromagnetic material, Appl. Phys. Express **13**, 123002 (2020).

[32] A. Brataas, Y. V. Nazarov, and G. E. W. Bauer, Spin-transport in multi-terminal normal metal-ferromagnet systems with non-collinear magnetizations, Eur. Phys. J. B **22**, 99 (2001).

[33] S. Zhang, P. M. Levy, and A. Fert, Mechanisms of spin-polarized current-driven magnetization switching, Phys. Rev. Lett. **88**, 236601 (2002).

[34] M. D. Stiles and A. Zangwill, Anatomy of spin-transfer torque, Phys. Rev. B **66**, 014407 (2002).

[35] I. M. Miron, K. Garello, G. Gaudin, P.-J. Zermatten, M. V. Costache, S. Auffret, S. Bandiera, B. Rodmacq, A. Schuhl, and P. Gambardella, Perpendicular switching of a single ferromagnetic layer induced by in-plane current injection, Nature (London) **476**, 189 (2011).

[36] J. Kim, J. Sinha, M. Hayashi, M. Yamanouchi, S. Fukami, T. Suzuki, S. Mitani, and H. Ohno, Layer thickness dependence of the current-induced effective field vector in Ta|CoFeB|MgO, Nat. Mater. **12**, 240 (2013).

[37] K. Garello, I. M. Miron, C. O. Avci, F. Freimuth, Y. Mokrousov, S. Blügel, S. Auffret, O. Boulle, G. Gaudin, and P. Gambardella, Symmetry and magnitude of spin-orbit torques in ferromagnetic heterostructures, Nat. Nanotechnol. **8**, 587 (2013).

[38] X. Qiu, P. Deorani, K. Narayanapillai, K.-S. Lee, K.-J. Lee, H.-W. Lee, and H. Yang, Angular and temperature dependence of current induced spin-orbit effective fields inTa/CoFeB/MgO nanowires, Sci. Rep. **4**, 4491 (2014).

[39] J. Kim, J. Sinha, S. Mitani, M. Hayashi, S. Takahashi, S. Maekawa, M. Yamanouchi, and H. Ohno, Anomalous temperature dependence of current-induced torques in CoFeB/MgO heterostructures with Ta-based underlayers, Phys. Rev. B **89**, 174424 (2014).

[40] Y.-C. Lau and M. Hayashi, Spin torque efficiency of Ta, W, and Pt in metallic bilayers evaluated by harmonic Hall and spin Hall magnetoreistance measurements, Jpn. J. Appl. Phys. **56**, 0802B5 (2017).

[41] Y. Shiokawa, E. Komura, Y. Ishitani, A. Tsumita, K. Suda, K. Hamanaka, T. Taniguchi, and T. Sasaki, Dependency of high-speed write properties on external magnetic field in spin-orbit torque in-plane magnetoresistance devices, Appl. Phys. Express **14**, 013001 (2021).

[42] W. Legrand, R. Ramaswamy, R. Mishra, and H. Yang, Coherent subnanosecond switching of perpendicularly magnetization by the fieldlike spin-orbit torque without an external magnetic field, Phys. Rev. Appl. **3**, 064012 (2015).

[43] T. Taniguchi, S. Mitani, and M. Hayashi, Critical current destabilizing perpendicular magnetization by the spin Hall effect, Phys. Rev. B **92**, 024428 (2015).

[44] W. F. Brown, Jr., Thermal fluctuations of a single-domain particle, Phys. Rev. **130**, 1677 (1963).

[45] T. Taniguchi, S. Isogami, S. Okame, K. Nakada, E. Komura, T. Sasaki, S. Mitani, and M. Hayashi, Probability of spin-orbit torque driven magnetization switching assisted by spin-transfer torque, Phys. Rev. B **108**, 134431 (2023).

[46] K. Garello, F. Yasin, S. Couet, L. Souriau, J. Swerts, S. Rao, S. V. Beek, W. Kim, E. Liu, S. Kundu, D. Tsvetanova, K. Croes, N. Jossart, E. Grimaldi, M. Baumgartner, D. Crotti, A. Fumémont, P. Gambardella, and G. S. Kar, SOT-MRAM 300 mm integration for low power and ultrafast embedded memories, in *2018 IEEE Symposium on VLSI Circuits, Honolulu, HI* (IEEE, Piscataway, NJ, 2018), pp. 81–82.

[47] M. Cubukcu, O. Boulle, N. Mikuszeit, C. Hamelin, T. Brächer, N. Lamard, M.-C. Cyrille, L. Buda-Prejbeanu, K. Garello, I. M. Miron, O. Klein, G. de Loubens, V. V. Naletov, J. Langer, B. Ocker, P. Gambardella, and G. Gaudin, Ultra-fast perpendicular spin-orbit torque MRAM, IEEE Trans. Magn. **54**, 9300204 (2018).

[48] Q. Shao, P. Li, L. Liu, H. Yang, S. Fukami, A. Razavi, H. Wu, K. Wang, F. Freimuth, Y. Mokrousov, M. D. Stiles, S. Emori, A. Hoffmann, J. Åkerman, K. Roy, J.-P. Wang, and S.-H. Yang, Roadmap of spin-orbit torques, IEEE Trans. Magn. **57**, 800439 (2021).

[49] K.-S. Lee, S.-W. Lee, B.-C. Min, and K.-J. Lee, Thermally activated switching of perpendicular magnet by spin-orbit spin torque, Appl. Phys. Lett. **104**, 072413 (2014).

[50] Y. Suzuki, A. A. Tulapurkar, and C. Chappert, in *Nanomagnetism and Spintronics*, edited by T. Shinjo (Elsevier, Amsterdam, 2009), Chap. 3.

[51] M. Matsumoto and T. Nishimura, Mersenne twister: A 623−Dimensionally equidistributed uniform pseudo-random number generator, ACM Trans. Model. Comput. Simul. **8**, 3 (1998).

[52] Y. Komoro, Weak order stochastic Runge-Kutta methods for commutative stochastic differential equations, J. Comput. Appl. Math. **203**, 57 (2007).

[53] J. Leliaert, J. Mulkers, J. D. Clercq, A. Coene, M. Dvornik, and B. V. Waeyenberge, Adaptively time stepping the stochastic Landau-Lifshitz-Gilbert equation at nonzero temperature: Implementation and validation inMuMax^3, AIP Adv. **7**, 125010 (2017).

[54] C. Abert, H. Sepehri-Amin, F. Bruckner, C. Vogler, M. Hayashi, and D. Suess, Back-hopping in spin-transfer-torque devices: Possible origin and countermeasures, Phys. Rev. Appl. **9**, 054010 (2018).

[55] C. Safranski and J. Z. Sun, Interface moment dynamics and its contribution to spin-transfer torque switching process in magnetic tunnel junctions, Phys. Rev. B **100**, 014435 (2019).

[56] H. Morise and S. Nakamura, Relaxing-precessional magnetization switching, J. Magn. Magn. Mater. **306**, 260 (2006).

[57] M. Oogane, T. Wakitani, S. Yakata, R. Yilgin, Y. Ando, A. Sakuma, and T. Miyazaki, Magnetic damping in ferromagnetic thin films, Jpn. J. Appl. Phys. **45**, 3889 (2006).